

Periodic driving of plasma turbulence

M. S. Baptista, I. L. Caldas, M. V. A. P. Heller, and A. A. Ferreira

Instituto de Física, Universidade de São Paulo, C. P. 66318, CEP 05315-970 São Paulo, S.P., Brazil

(Received 16 December 2002; accepted 27 January 2003)

Tools to characterize three important characteristics of turbulence are proposed: Structures-within-structures, intermittent amplitude bursting, and turbulence complexity. These tools are applied to show that the injection of a rf wave into the plasma confined on the Tokamak Chauffage Alfvén Bresilién (TCABR) [R. M. O. Galvao, V. Bellintani, Jr., R. D. Bengtson *et al.*, Plasma Phys. Controlled Fusion **43**, A299 (2001)] decreases plasma edge turbulence, although not completely destroy it, by destroying the only two types of time structures found in the data. Both structures present multiscaling spectra, with infinitely many possible scalings. So, according to this analysis, complexity of this turbulence is mainly due to the multiscaling character of the oscillations.

© 2003 American Institute of Physics. [DOI: 10.1063/1.1561612]

I. INTRODUCTION

Turbulence is among one of the most interesting phenomenon in physics, very common in life and yet not completely understood.^{1–3} Some important tools contribute much for a good understanding of turbulence: The Reynolds number⁴ which can be used to measure the level of turbulence, the scaling between the diffusivity of relative particles and the length scale of a fluid,⁵ and the strong formal definition of turbulence based on relative diffusion in terms of the averaged relative velocities of pairs of particles.^{6,7} In this work we propose new tools that introduce a statistical dynamical description of turbulence that can improve the understanding of turbulence.

We study magnetohydrodynamic plasma turbulence as described in Ref. 8. The use of only traditional plasma physics, as pointed out in Ref. 9, is not sufficient to explain the experiments in fusion plasma confinement, as, for example, the observed particle transport.¹⁰ So, like in Refs. 11–15, we propose new tools to improve the understanding of plasma turbulence, which should be, in principle, applicable to any type of turbulent system, once plasma turbulence seems to have all the characteristics of fluid turbulence. One of the interests in studying plasma edge turbulence is that, in the case one wants to construct a controlled fusion reactor fed by plasma, turbulence should be avoided, once it is responsible to increase particle transport that drives particles out of the plasma. Although the main reason of injecting rf Alfvén wave into the plasma cavity is to increase plasma temperature, our intention, in this paper, is to understand, from the dynamical point of view, the effect this wave has on the structures present in the plasma edge turbulence, and its consequences for the level of it.

For that, we propose tools that identify modifications in the characteristics of three properties of turbulence. *The structures-within-structures acting on each other in different time scales*, the typical *intermittent amplitude-bursting of the turbulent oscillations*, and its *complexity* (being quantified by the amount of predictability one can get from the data). To characterize the action of the structures acting on different

time scales, we look into self-similarities in the data. We further adapt the multifractal formalism proposed in Ref. 16 for its application in time series. That will give us all the possible self-similar exponents in the time series, which will enable us to fully characterize the multiscaling of the data. To characterize the intermittent amplitude-bursting, we check for phase synchronization between positive-peak and negative-peak amplitudes, and to characterize its complexity we calculate the inverse of the N-Gramm entropy, of a symbolic sequence obtained from the data, which measures the amount of predictability obtained observing a certain amount of data.

In our proposed time multiscaling analysis we can identify clearly only two structures. One is a low-period *small structure* (with time dimensions of less than 20 μ s), and the other is a high-period *large structure* (with time dimensions higher than 200 μ s). Considering all the other analysis, our main result, on the acting of the wave, is that the wave acts destructively in both structures.

The contents of the paper are as follows. In Sec. II, we describe the experiment as well as the turbulent data. In Sec. III, we describe the proposed time multiscaling formalism which unravels the structures present in the data. In Sec. IV, we show that the phase synchronization between the positive and negative peaks gets stronger when the wave is introduced. In Sec. V, we make a symbolic analysis of the data, showing the increase of the predictability when the wave is injected. Finally, in Sec. VI, we present the conclusions.

II. THE DATA

The experiment is performed in a hydrogen plasma in the Tokamak Chauffage Alfvén Bresilién (TCABR)¹⁷ (major radius $R_0 = 0.61$ m and minor radius $a = 0.18$ m). The plasma current I_p is 100 kA, the current duration 100 ms, the toroidal magnetic field B_t is 1.1 T. In order to study turbulence changes introduced by Alfvén wave injection, we keep the rf power during 10 ms in the range of 40 kW at 3.6 MHz, for excitation of modes $m/n = 1/4$, where m and n are the poloidal and toroidal mode numbers, respectively. The data are

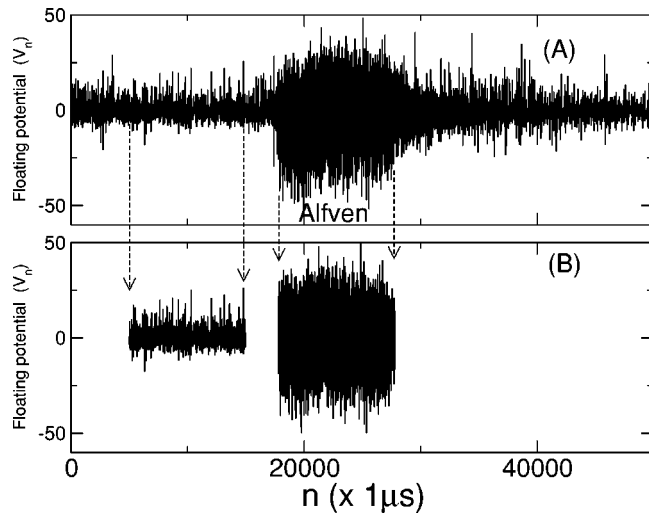


FIG. 1. (A) Floating potential for the complete discharge and (B) the selected pieces (without and with Alfvén wave injection) of the data for the analysis. The sampling time is $1 \mu\text{s}$.

collected with a multi-pin probe (for more details see Ref. 12) that measures the fluctuations on the floating potential in the scrape-off layer (outer region of the plasma chamber), V_n . Figure 1 shows the floating potential for one complete discharge and for selected intervals.

The variable of analysis is the floating potential difference, R_n , defined as

$$R_n = (V_{n+1} - V_n) / \sigma, \quad (1)$$

where R_n is normalized by the standard deviation σ of V_n . This variable is shown in Fig. 2 without (A) and with the rf injection (B). The intermittent peak-to-peak bursting is more evident without rf injection. The size of the data to be analyzed, i.e., the maximum value for n is $N = 10000$.

In Fig. 3 we show the probability distribution function (PDF) of R_n without (A) and with the wave injection (B). Without the wave, $\rho(R_n)$ has a Poisson decay and large amplitude events indicating a power-law tail, as it is expected

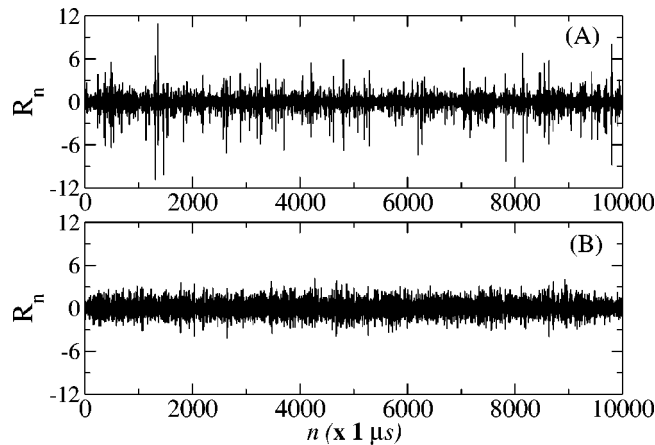


FIG. 2. R_n without wave (A) and with wave (B). Intermittent peak-to-peak bursting is reduced when the wave is injected.

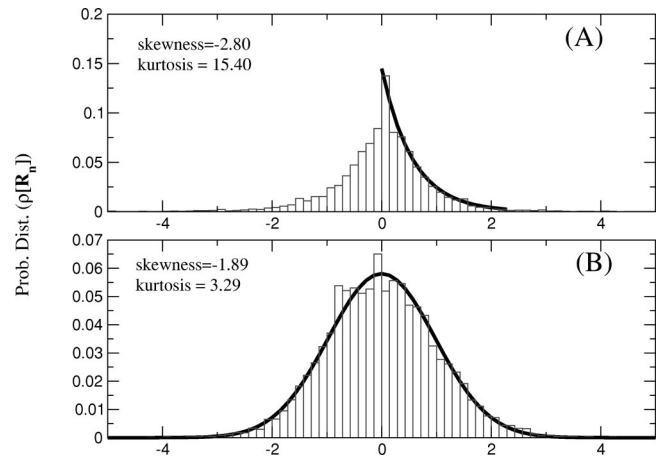


FIG. 3. Probability distribution for the data without (A) Alfvén wave and with (B), shown in Fig. 1 (B).

from the measured plasma turbulence.^{11,13–15} With the wave, the distribution kurtosis changes to 3.29, a value near the one obtained for a Gaussian distribution.

III. STRUCTURES-WITHIN-STRUCTURES

Turbulence has organized (coherent) structures that are observed both in time and in space. These structures can be characterized by either their time scales or space scales. Our work is dedicated to identify such structures in the time domain. That is done finding distributions of floating potential fluctuations that are self-similar for a given time interval. Thus, we search for self-similar patterns in the data, as we change the time scale within which we observe the fluctuations, i.e., we search for a scaling of the probability distribution of the floating potential as we change the time scale of the observation.

Due to the short duration of the discharge, instead of observing the floating potential each m samplings, we average the signal within overlapping time windows, j , of size m . Then, we introduce an average positive value of the floating potential over different time scales

$$\Gamma_j(m) = \frac{1}{k} \sum_{i=1}^k R_{i,j}^+, \quad (2)$$

where $R_{i,j}^+$ are the k values bigger than the average value of R_n within the window j (with m points and $k < m$). Once we work with overlapping time windows, for a chosen m we can have $N - m$ windows. The reason for introducing the variable $\Gamma_j(m)$ in Eq. (2) is that, for the plasma edge turbulence, the PDF of this variable is a Poisson-type and should be characterized by its average positive value as shown in Refs. 11 and 13–15.

A PDF $\rho[\Gamma_j(m)]$ is said to be self-similar if $\rho[\Gamma_j(m)] \propto m^D \rho[m^{-D} \Gamma_j(m)]$ (see Refs. 18–20), where D is the self-similar parameter. A PDF is defined to be multiscaling if $\rho[\Gamma_j(m)^q] \propto m^{D_q} \rho[m^{-D_q} \Gamma_j(m)]$, where D_q varies nontrivially with q , and $q \in \mathcal{R}$. For simplicity, instead of working with the properties of the distribution $\rho[\Gamma_j(m)^q]$, we work with the mean $\langle \Gamma_j(m)^q \rangle = [1/(N - m)] \sum_{j=1}^{N-m} \Gamma_j(m)^q$. This mean can be associated to the width of the distribution of

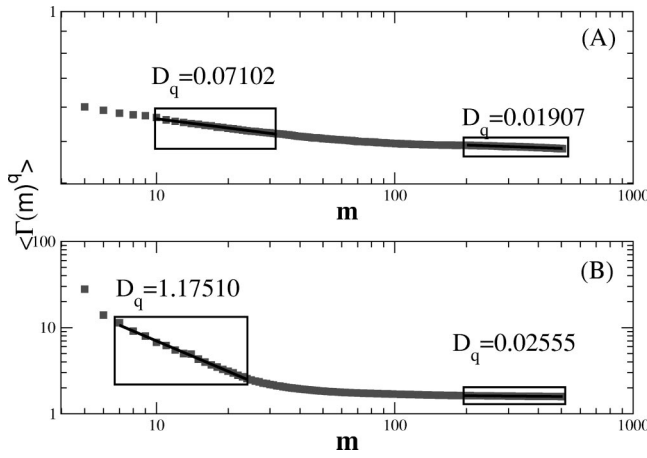


FIG. 4. $\langle \Gamma(m)^q \rangle$ for the data without wave injection (A) and with wave injection (B) with respect to m , for $q = -3.0$. Two self-similar regions appear. One in a short time interval region (small structure) and the other for large time windows (large structures).

positive values of $R_n(m)$ defined as $(V_{n+m} - V_n)/\sigma$. A consequence of having a multiscaling self-similar PDF is that all the characteristics of the PDF are also multiscaling self-similar, and therefore

$$\langle \Gamma_j(m)^q \rangle \propto m^{-D_q}, \tag{3}$$

where D_q is the generalized scaling characterizing the evolution of the q -order moment of the distribution $\rho[\Gamma_j(m)^q]$. Note that $D_q = D_1 \times q$ for a one-scaling probability distribution $\rho[\Gamma_j(m)]$, and $D_q \neq D_1 \times q$, for a multiscaling distribution. Moreover, the exponent D_q is equivalent to $\tau(q)$, first introduced in Ref. 21, later in Refs. 22 and 23. In Ref. 23, given a measure $\chi(m, q)$ of a set, $\tau(q)$ is the exponent $\chi(m, q) \propto \epsilon^{\tau(q)}$, where ϵ is some small interval in the set.

So, to understand how the q th moment of $R_n(m)$ evolves with m we show in Fig. 4 how $\langle \Gamma_j(m)^q \rangle$ evolves with m , where we choose $q = -3.0$. We see that for both data (with and without the wave injection) there are mainly two regions of self-similarity, for all q , which basically means that Eq. (3) is valid for these time domains. Once, Eq. (3) is a power-law, it preserves the form within each time domains. Thus, the dynamics responsible for such invariance can be fully characterized by the exponents D_q . Such dynamics are the result of some time structure.

Although the knowledge of wave number power spectrum requires measurements in different positions, there are correlations between the space and time power spectra of structures propagating inside the plasma. In this sense the time scales of structures found in this work could give some insight of space scales of these structures. In fact, as also described in Ref. 20, there is a connection between the structures found in time domain (self-similar regions) and the structures present in the space domain. So, the short time self-similar regimes are consequence of the existence of high-frequency structures that are also small structures within the space domain. Similarly, the large time self-similar regimes are consequence of low-frequency structures

that are also large structures in the space domain. Therefore, identifying the time scale of the existing structures means to identify the space-scale of these structures.

Thus, in Fig. 4 we show the value of $\langle \Gamma(m)^q \rangle$ for the data without wave injection (A) and with wave injection (B). One can see two types of structures. One is a short-period (with time dimensions smaller than $30 \mu s$) that we associate to *small structure* in the space domain, and the other is a high-period (with time dimensions higher than $100 \mu s$) that we associate to a *large structure* in the time domain. These two time regions vary slightly in length (windows of length m) and position as we change q , and they are associated with two types of structures found in the data.

A. Generalized local and global time exponents

To reveal how nonlinear D_q is with respect to q , and therefore, to check if $\langle \Gamma(m)^q \rangle$ is either mono or multifractal, we just analyze if the derivative of D_q with respect to q (α), is either constant or a nontrivial curve

$$\alpha = \frac{dD_q}{dq}. \tag{4}$$

The exponent α is equivalent to the singularity exponent α_j introduced in Refs. 16, 25, and 26 or to the ‘‘pointwise dimension’’ (see a discussion of this equivalence in Ref. 24), which is a spatially local exponent. So, like in those works, we also consider α to be a local measure, that in our case is a measure within a localized time windows. Differently from the works of Refs. 16, 25, and 26, in which the local exponent is calculated as a local space interval shrinks to zero, in our time formalism we interpret α as a measure of a particular window j , as its size m increases.

We also define the exponent f_α by

$$f_\alpha = q\alpha - D_q, \tag{5}$$

which measures higher order terms in the expansion of D_q , that differs from $(dD_q/dq)q$. So, it measures how many different scalings we have in $\langle \Gamma(m)^q \rangle$. For example, if D_q is monofractal, $f_\alpha = 0$ for all α , and therefore, is punctual and monofractal. In the case we have multifractal system, f_α is a curve with respect to α , and we have an infinite spectrum of values. The interval of α values for which f_α exists is a measure of the number of different scalings the system have. So, the exponent f_α is the characteristic exponent of the set of values α , and the curve of f_α versus α we call spectra f_α .

In the multifractal formalism of Ref. 16, assuming that $\Gamma(m)$ is a summation over the probabilities of finding points, within some interval, from a given set of points, D_0 is the capacity dimension,²⁷ equivalent to the Hausdorff dimension.²⁸ These metric dimensions are also known by the generic term of fractal dimension coined by Mandelbrot in Ref. 29 referring to the Hausdorff dimension of some measured variable, meaning that such measurement could be globally characterized by a noninteger power-law exponent. D_1 is the information dimension,³⁰ equivalent to the pointwise dimension introduced in Ref. 31. In the present proposition, D_q should be understood as the generalized exponent of the q -moments of the time measurement $\Gamma(m)$, which in this

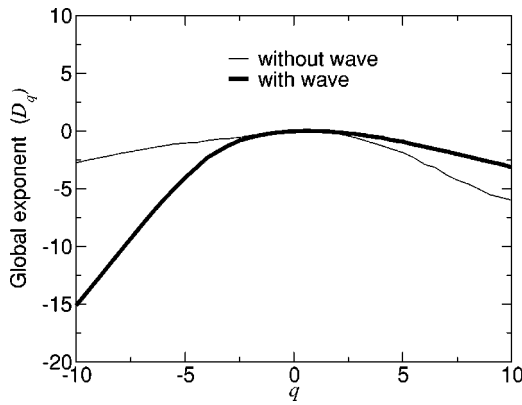


FIG. 5. Global exponent $D_q(q)$ with respect to q , showing the average scalings for large time, $m > 200$.

case characterizes the probability distribution $\rho[\Gamma(m)^q]$. So, while D_q in Ref. 23 describes spatial properties of points in a set, in the present work D_q describes the time evolution of the distribution of the ensemble $\sum_{j=1}^{N-m} \Gamma_j(m)^q$. Similarly to the work of Ref. 23, where D_q characterizes global and universal invariants of the set, in the present work D_q describes global invariants of the distribution of this ensemble. To go from this formalism to the one proposed in the generalized dimensions, Γ should describe probabilities densities of the data as the space shrinks to zero. In the present case, the space in which the data live does not have to be defined. This is attracting to turbulent data analysis, because the space of turbulent systems are usually considered to be either unknown, or higher dimensional, and thus difficult to deal with. We refer to D_q as the *generalized global time exponent*.

B. Time multi-exponents analysis of the data

Following, we describe results of the time multiscaling exponents analysis of the data, for large m that we choose it to be $m > 200$. Therefore, such analysis tries to understand what happens to the large time-domain structures, associated with the large space-domain structures. In that case, the generalized global exponent D_q is shown in Fig. 5 with and without the wave, for q within the interval $[-10, 10]$. These exponents are obtained by fitting the curve $\langle \Gamma(m) \rangle$ versus m . The existence of such continuous and smooth curve for D_q versus q shows that the data are self-similar for that time domain, and consequently, Eq. (3) is valid. From this figure, with and without wave the data is self-similar. We find multi-similarity in both data, as one can check by the existence of a nonlinear curve of α with respect to q , shown in Fig. 6. Finally, a measurement of how much multi-similar the data is given by the interval range (bandwidth) for which the function f_α exists. One can see in Fig. 7 that, for the data with wave, the bandwidth in the α variable is smaller than without the wave. That means that the wave destroy many structures that were responsible for making the data to present a larger number of exponents, and consequently a higher complexity curve of α versus q .

Another range of m we find self-similarity in the function $\langle \Gamma(m) \rangle$ is for small values of m , that is $m < 20$. The results are shown in Figs. 8 and 9, and they are similar to the

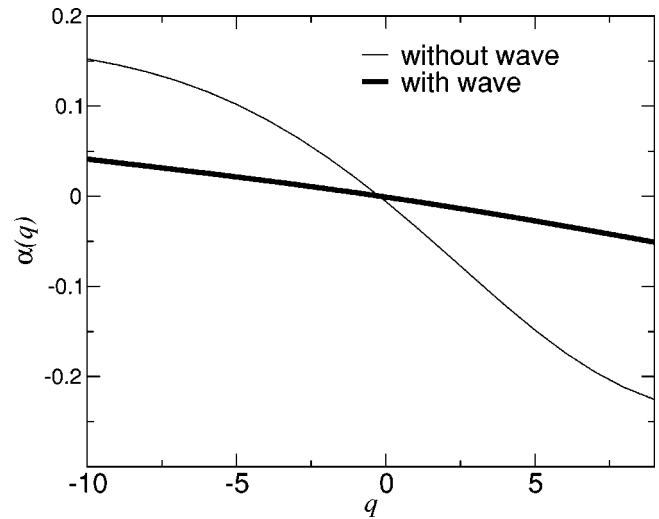


FIG. 6. Local exponent $\alpha(q)$ with respect to q , for large time, $m > 200$.

ones presented in Figs. 5–7. In Figs. 8–10, we consider only positive values of q due to numerical problems that arise in the sum of Eq. (2) if $q < 0$, for $m < 20$. It is worth mentioning that the bandwidths (for both data sets, with and without the wave) of α values for this time domain is larger than the ones found in the large time-domain (Figs. 5–7). That means that the small structures, should be more complex than the large structures.

IV. PEAK-TO-PEAK SYNCHRONIZATION

Turbulence is characterized by an intermittent behavior between explosions of large amplitude and medium oscillations. Studying the phase between turbulent peak-to-peak oscillations enables us to both characterize turbulence and to understand the effect of the wave injected on the plasma.

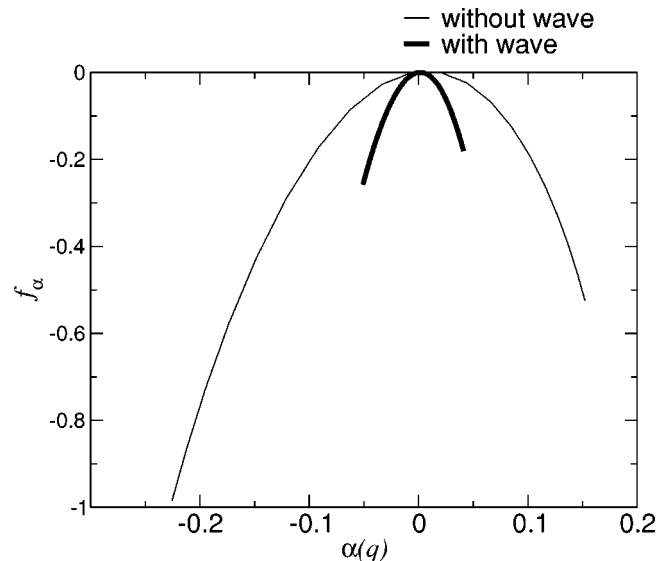


FIG. 7. f_α spectra for large time, $m > 200$. The wave is responsible for a shrinkage of the spectra which means that the large structures are being destroyed.

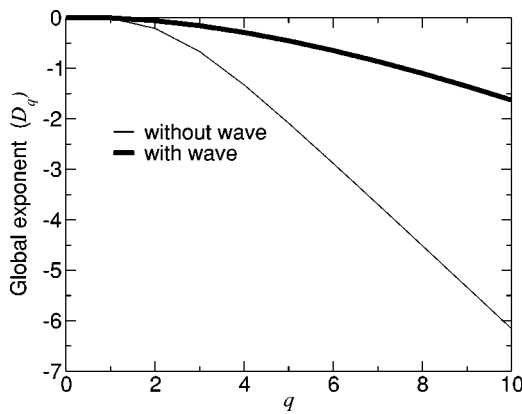


FIG. 8. Global exponent $D_q(q)$ with respect to q , showing the average scalings for short time, $m < 20$. Only positive values of q are considered.

For that, we analyze the standard deviation σ of the probability distribution, $\rho[\epsilon(t)]$, for the difference $\epsilon(t)$

$$\epsilon(t) = |\phi_1(t) - \phi_2(t)| \bmod \pi, \quad (6)$$

where $\phi_1(t)$ is the phase of the series $s^+(t)$,³² constructed by the values of R_n bigger than $\delta/2$, and $\phi_2(t)$ is the phase of the series $s^-(t)$, constructed by the values of R_n smaller than $-\delta/2$. We show in Fig. 11 an example of $s^+(t)$ and $s^-(t)$, and in Fig. 12 as σ changes with the gap δ . Once turbulence is characterized by the existence of a sum of an infinite number of phases, we do the same analysis leading to Fig. 12, for R_n as it is smoothed out by running averages within windows of size T ; here $T < 20$. With that procedure we want to eliminate from the data possible fast oscillations which could affect the reliance of the phase analysis. The result is similar to the one obtained without the running average, and thus, we can state that the wave is responsible for synchronizing the peak-to-peak oscillations. In fact, we observe that the data with the wave do not present large amplitude bursting, as one can see from Fig. 2.

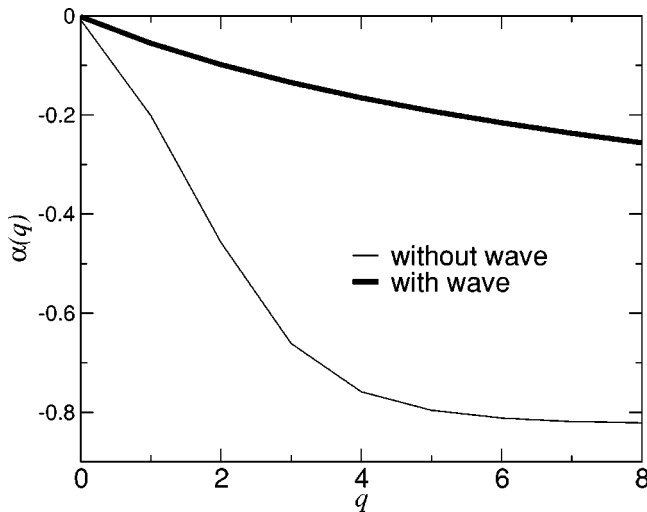


FIG. 9. Local exponent $\alpha(q)$ with respect to q , for short time, $m < 20$. Only positive values of q are considered.

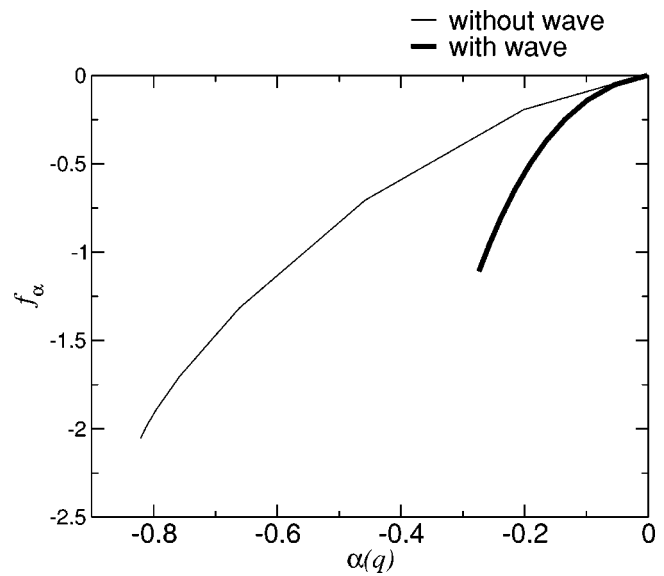


FIG. 10. f_α spectra for short time, $m < 20$. The wave is responsible for a shrinkage of the spectra which means that the small structures are being destroyed. Only positive values of q are considered.

V. SYMBOLIC MAPPING, STRUCTURES-WITHIN-STRUCTURES, REGULARITY, AND PREDICTABILITY

In a symbolic analysis we do not work with windows of very large m . Instead, we symbolize R_n by associating symbols to its values, working with small-length time-windows, and so, generating short length sequences of symbols. That type of analysis should be used to search for structures for short-time windows. The structures found in this symbolic analysis should be considered to be the ones that are characterized, in the previous sections, by the global and local exponent, for small m . So, we make a microscopical search for structures within short-time windows of $12 \mu s$ ($m = 12$). With this analysis we also find two types of symbolic structures, which we classify as large and small. Therefore, this result should be a consequence of the structures-within-structures characteristic of turbulence. So, we symbolize the data with the symbol “0,” if R_n is negative, and “1” if it is

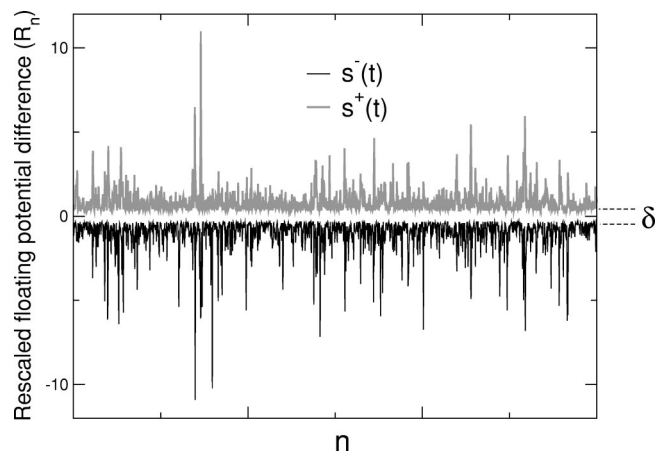


FIG. 11. $s^+(t)$ are the values of R_n which are bigger than $\delta/2$, and $s^-(t)$ are the values of R_n which are smaller than $-\delta/2$.

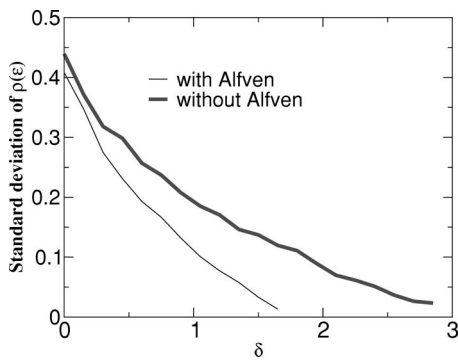


FIG. 12. Dependence of $\sigma[\epsilon]$ on δ for the plasma with and without the Alfvén wave. The wave injection makes $\sigma[\epsilon(t)]$ to get smaller, which means that the phase synchronization between the positive and the negative oscillations increases.

positive. We construct the symbolic sequence S_n , that is separated in overlapping regions of 12 symbols each. To treat this problem in a Cartesian space, we convert each group, i , of 12 symbols, that we refer to it as a 12-bit sequence, into a decimal, d_i , by using the decimal-binary conversion rule: $d_i = \sum_{j=1}^{12} S_j \times 2^{(12-j)}$. From the decimals d_i , we construct the symbolic mapping, d_i versus d_{i+1} , shown in Figs. 13(A) and 13(B), where Fig. 13(A) is for the discharge without the wave injection, and Fig. 13(B) with the wave. The blank regions of Fig. 13(B) corresponds to forbidden sequences, and are, in its majority, composed by repeating sequences of the same symbol. Therefore, small-lengthed cyclic sequences of bits as “01010101 . . .” are very common. These particular symbolic sequences represent a patterned time oscillation. Symbolic sequences like this previous one, with typically low-period patterns, are a consequence of a low-period time oscillation, and therefore high frequency, which as done previously, we believe is consequence of a small spatial structure. On the other hand, long-period symbolic patterns, like for example “111111111111,” or “000000111111,” are a consequence of a large-period time oscillation, which we be-

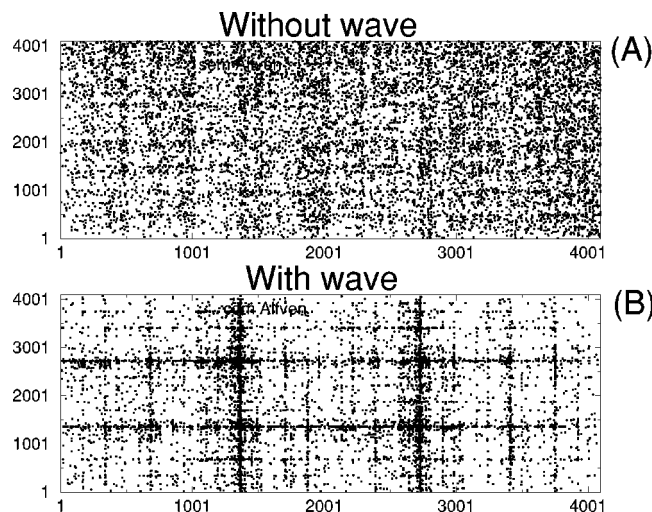


FIG. 13. The symbolic map with (A) and without (B) the wave injection. Blank regions in (B) represent the symbolic large structures that are destroyed by the wave injection.

lieve to be a consequence of a large spatial structure. These symbolic large structures are represented by d_j decimal which correspond to horizontal and vertical lines, positioned at 1, 1024, 2048, 3076, and 4096. These lines positions are in the blank regions of the mapping. So, patterns with long-period symbolic structures are unlikely to be found when the wave is injected in the plasma. Therefore, although the wave acts destructively in the small time-structures ($m < 20$) as it was observed in the previous sections, symbolic low-period time structures seems not to be so affected by the wave as it is the case for symbolic large-period time structures. As a consequence, the remaining α bandwidth after the wave injection, in Fig. 10, should be mainly due to this symbolic low-period patterns also consequence of high-frequency time oscillations.

More powerful than only detecting patterns in the symbolic sequences, the symbolic analysis can also give us an idea of the complexity of the data from its entropy and predictability. For this complexity quantification, we follow the treatment described in Ref. 33. So, the Shannon entropy³⁴ of words of length m are given by

$$H_m = - \sum p_i^{(m)} \log p_i^{(m)}, \tag{7}$$

where the summation has to be carried out over all words with $p_i^{(m)} > 0$. The entropies H_m measure the amount of information contained in a word of length m . From Eq. (7) we define the conditional (dynamic) entropy h_m as the average information necessary to predict the next symbol, given the preceding m symbols, by

$$h_m = H_{m+1} - H_m, \tag{8}$$

with $h_0 = H_1$. The entropy of the source is the average information content of one symbol, or the information necessary to predict the next symbol when being informed about the complete pre-history of the system

$$h = \lim_{n \rightarrow \infty} h_m = \lim_{m \rightarrow \infty} \frac{H_m}{m}. \tag{9}$$

Note that when Eq. (9) is used to calculate the source entropy of a symbolic sequence generated from a dynamical system, with a symbolization of the trajectory through a Markov partition, then, Eq. (9) is the Kolmogorov–Sinai entropy of the trajectory, as shown in Ref. 35. In the case the Kolmogorov–Sinai is positive, that means the trajectory is chaotic. In the present analysis, however, we interpret the finding of a h positive as a measure of complexity, i.e., the more positive h is, the more complex are the data. While Eq. (9) should be used to have a global characterization of complexity, Eq. (8) should be used to have an “instantaneous” characterization of complexity. From the decay of h_m with respect to m we can understand how much order (fast decay) or disorder (slow decay) the data have. The maximum value h can assume is $\ln(2)$.

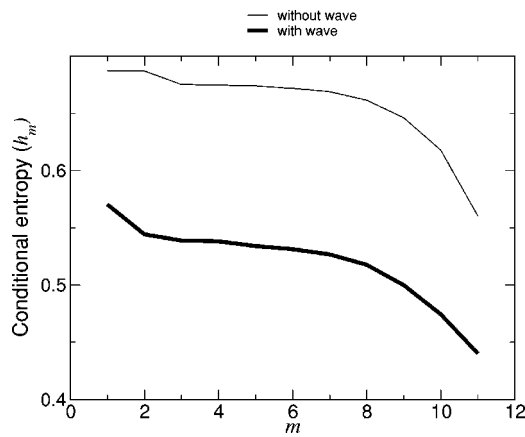


FIG. 14. Conditional entropy for data with (A) and without (B) the wave. The faster decay of this entropy with respect to m indicates that the wave injection introduces regularity and predictability in turbulence.

The ability to predict, \mathcal{P} , is defined as³³

$$\mathcal{P} = 1 - h_m. \tag{10}$$

So, we obtain $h = 0.53$ for data with the wave and $h = 0.66$ for data without the wave. Note that the value for h , for the data without the wave, is close to the maximum value, which agrees with the believed random-like character of turbulence.

In Fig. 14 we show the conditional entropy which is smaller for all m for the data with the wave. That means, the uncertainty of the bit g , analyzing the previous $g - m$ symbols in the sequences is smaller with the injection of the wave. Also, the slow decay for small m shows that the data have a very complex characteristic, nontypical of chaotic system, that have a faster decay. Finally, in Fig. 15 we show the ability of prediction for a given m and we see that the wave introduces into the turbulent data more predictability. In Figs. 14 and 15, the abrupt change in the slope of the functions for m higher than 8 is due to the insufficient number of experimental data.

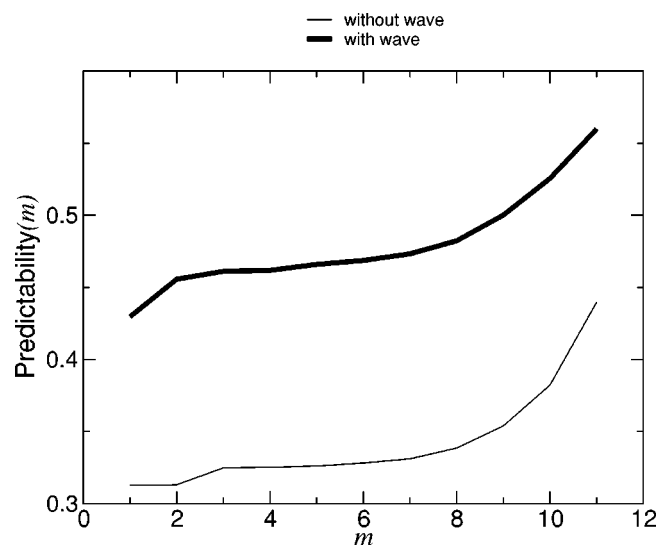


FIG. 15. Predictability for data with (A) and without (B) the wave. Clearly, the wave injection increases the predictability of the data.

VI. CONCLUSION

The wave injection decreases turbulence by destroying both the large (time windows of $[200,500]\mu s$) and the low period structures (time windows of $[1,20]\mu s$). However, for the low-period structures we have observed by the symbolic analysis that the higher-frequency time oscillations are more resistant than the lower-frequency time oscillations in the presence of the wave injection. A direct consequence of the decrease of the turbulence level, due to the wave injection, is the increase in the regularity and predictability of the data. Regularity is indicated by the smoothing of the data, phase synchronization between the positive and negative peak oscillations, the smaller value of the source entropy, and the faster decay of the conditional entropy.

These conclusions are a consequence of an integrated comparison of the results of our proposed tools of analysis which identifies the time changes caused by the wave in the structures present in the data. With the visual inspection of the normalized data and the phase difference between peak-to-peak oscillations we show the plasma edge turbulence has a typical peak-to-peak intermittent oscillation (coupling between the *large structure* and the *small structure*) which is destroyed by the wave, resulting in more uniform data. The probability distribution for the data without the wave injection is a typical turbulent Poisson-type distribution^{11,13-15} that with the wave turns into a Gaussian-type. However, as shown by our local and global multiscalings analysis, there are two time self-similar regions for both data. Which means that independently of the distribution found, its time evolution happens according to multiscalings rules, and therefore, not randomly. Finally, with the symbolic analysis, we show that the wave creates forbidden zones in the symbolic mapping which means that symbolic structures are destroyed.

Therefore, our tools of analysis not only give us a good understanding of the driving of resonant rf wave in the plasma edge turbulence, but also give a criteria for the characterization of the turbulent level. The higher turbulence is, the higher peak-to-peak intermittent oscillations are, the wider the f_α spectra are, the less phase-synchronized the positive and negative peak oscillations are, the more dense is the symbolic mapping is, and the more unpredictable the data are. Finally, our tools could be used in a real-time experiment to detect if a flow is about to become more turbulent, just by showing that the measured quantities proposed with these tools are changing in time, heading to values that characterize a stronger turbulent state.

The finding of only two main structures, on the analyzed data, could be related with the theory described in Ref. 36 which describes the onset of turbulence from the breakup of a two-frequency torus.

ACKNOWLEDGMENTS

This work was supported by Fundação de Amparo à Pesquisa do Estado de São Paulo (FAPESP) and Conselho Nacional de Desenvolvimento Científico e Tecnológico (CNPq).

- ¹L. D. Landau and E. M. Lifshitz, *Fluid Mechanics* (Pergamon, New York, 1987).
- ²J. Argyris, G. Faust, and M. Haase, *An Exploration of Chaos* (North-Holland, New York, 1994).
- ³P. Moin and J. Kim, *Sci. Am.* **276** (1), 46 (1997).
- ⁴The Reynolds number is defined as the upstream velocity of the fluid times the frontal height of the obstacle in the fluid divided by the viscosity.
- ⁵L. F. Richardson, *Proc. R. Soc. London, Ser. A* **101**, 709 (1926).
- ⁶A. N. Kolmogorov, *Dokl. Akad. Nauk SSSR* **30**, 3201 (1941).
- ⁷A. N. Kolmogorov (translation by V. Levin), *Proc. R. Soc. London, Ser. A* **434**, 9 (1991).
- ⁸A. Yoshizawa, S.-I. Itoh, and N. Yokoi, *Plasma Phys. Controlled Fusion* **43**, R1 (2001).
- ⁹R. D. Hazeltine and S. C. Prager, *Phys. Today* **55**(7), 30 (2002).
- ¹⁰P. Beyer and S. Benkadda, *Chaos* **11**, 774 (2001).
- ¹¹M. S. Baptista, I. L. Caldas, M. S. Baptista, C. S. Baptista, A. A. Ferreira, and M. V. A. P. Heller, *Physica A* **287**, 91 (2000).
- ¹²A. A. Ferreira, M. V. A. P. Heller, and I. L. Caldas, *Phys. Plasmas* **7**, 3567 (2000).
- ¹³M. S. Baptista, I. L. Caldas, M. S. Baptista, C. S. Baptista, A. A. Ferreira, and M. V. A. P. Heller, *Physica A* **301**, 150 (2002).
- ¹⁴M. S. Baptista, I. L. Caldas, M. V. A. P. Heller, and A. A. Ferreira, *Phys. Plasmas* **8**, 4455 (2001).
- ¹⁵M. S. Baptista, I. L. Caldas, M. V. A. P. Heller, and A. A. Ferreira, *Physica A* **301**, 150 (2002).
- ¹⁶T. C. Halsey, M. H. Jensen, L. P. Kadanoff, I. Procaccia, and B. I. Shraiman, *Phys. Rev. A* **33**, 1141 (1986).
- ¹⁷R. M. O. Galvao, V. Bellintani, Jr., R. D. Bengtson *et al.*, *Plasma Phys. Controlled Fusion* **43**, A299 (2001).
- ¹⁸B. B. Mandelbrot, *The Fractal Geometry of Nature* (Freeman, New York, 1982).
- ¹⁹A.-L. Barabási, P. Szépfalussy, and T. Vicsek, *Physica A* **178**, 17 (1991); A.-L. Barabási and T. Vicsek, *Phys. Rev. A* **44**, 2730 (1991).
- ²⁰B. A. Carreras, B. van Milligen, C. Hidalgo *et al.*, *Phys. Rev. Lett.* **83**, 3653 (1999); B. A. Carreras, B. Ph. van Milligen, M. A. Pedrosa *et al.*, *Phys. Plasmas* **5**, 3632 (1998); B. A. Carreras, V. E. Lynch, D. E. Newman *et al.*, *ibid.* **7**, 3278 (2000).
- ²¹A. N. Kolmogorov, *J. Fluid Mech.* **13**, 82 (1962).
- ²²E. A. Novikov, *Dokl. Akad. Nauk SSSR* **184**, 1072 (1969).
- ²³H. G. E. Hentschel and I. Procaccia, *Physica D* **8**, 435 (1983).
- ²⁴E. Ott, *Chaos in Dynamical Systems* (Cambridge University Press, New York, 1994).
- ²⁵R. Benzi, G. Paladin, G. Parisi, and A. Vulpiani, *J. Phys. A* **17**, 3521 (1984).
- ²⁶U. Frisch and G. Parisi, *Turbulence and Predictability in Geophysical Fluid Dynamics and Climate Dynamics* (North-Holland, New York, 1985).
- ²⁷A. N. Kolmogorov, *Dokl. Akad. Nauk SSSR* **119**, 861 (1958).
- ²⁸F. Hausdorff, *Math. Ann.* **79**, 157 (1918).
- ²⁹B. B. Mandelbrot, *Fractals, Form, Chance, and Dimension* (Freeman, San Francisco, 1977).
- ³⁰J. Balatoni and A. Renyi, *Publ. Math. Inst. Hungarian Acad. Sci.* **1**, 9 (1956).
- ³¹J. D. Farmer, E. Ott, and J. A. Yorke, *Physica D* **7**, 153 (1983).
- ³²P. Tass, M. G. Roseblum, J. Weule, J. Kurths *et al.*, *Phys. Rev. Lett.* **81**, 3291 (1998).
- ³³R. Steuer, L. Molgedey, W. Ebeling, and M. A. Jiménez-Montaño, *Eur. Phys. J. B* **19**, 165 (2001); W. Ebeling, R. Steuer, and M. R. Titchener, *Stochastic and Dynamics* **1**, 45 (2001); L. Molgedey and W. Ebeling, *Eur. Phys. J. B* **15**, 733 (2000).
- ³⁴C. E. Shannon, *Bell Syst. Tech. J.* **27**, 379 (1948).
- ³⁵M. S. Baptista, E. E. Macau, and C. Grebogi, *Chaos* **13**, 145 (2003).
- ³⁶D. Ruelle and F. Takens, *Commun. Math. Phys.* **20**, 167 (1971).